

Galactic Center Studies with CTA-LST-1

Shotaro Abe^{a,*}, Yoshiki Ohtani^a, Marcel Strzys^a, Masahiro Teshima^{a,b}, and Ievgen Vovk^a for the CTA-LST Project

^a*Institute for Cosmic Ray Research,
Kashiwa-no-ha 5-1-5, Kashiwa-shi, Chiba, Japan.*

^b*Max-Planck-Institut für Physik,
Föhringer Ring 6, 80805, München, Germany.*

E-mail: shotaro@icrr.u-tokyo.ac.jp

The Galactic Center region is known to host a wide variety of very-high-energy gamma-ray sources. In 2018 the prototype of the Large-Sized Telescope (LST-1) for CTA was inaugurated, and has been regularly observing the Galactic Center since 2021. To observe the Galactic Center in the southern sky, LST-1, located in the Northern hemisphere, requires an observation mode at a low telescope elevation. In this study, we assessed the performance of LST-1 at the large zenith angle, based both on simulations and observational data for the standard candle Crab Nebula. Analyzing LST-1 data from the Galactic Center observations, we obtained the spectral energy distributions of Sagittarius A* and G0.9+0.1, which were comparable with the results from the current imaging atmospheric Cherenkov telescopes, with a broad energy coverage owing to the large-zenith-angle observation and the low energy threshold of LST-1.

The 38th International Cosmic Ray Conference (ICRC2023)
26 July – 3 August, 2023
Nagoya, Japan



*Speaker

1. Introduction

The central region of the Milky Way Galaxy has been intensively explored through very-high-energy (VHE) gamma rays by the current imaging atmospheric Cherenkov telescopes (IACTs). As compared with an extragalactic source, the proximity allows for an investigation of the morphology, for the angular resolution of $\lesssim 0.1$ deg for a typical IACT system, of extreme phenomena around the supermassive black hole Sagittarius A* (Sgr A*).

H.E.S.S. reported diffuse emission spanning hundreds of parsecs with a power-law energy spectrum without a cut-off and a $1/r$ dependence of the radial profile of the cosmic-ray density, which indicate hadron acceleration in the vicinity of Sgr A* [1]. MAGIC presented, however, the spectral energy distribution (SED) of the diffuse emission with a 2σ deviation from the power law, suggesting a cut-off around 20 TeV, and argued that an uncertainty of the gas distribution makes a non-negligible influence on the derivation of the radial profile [2].

Moreover, VHE gamma rays from the Galactic Center might serve as a good messenger of annihilation or decay of the Weakly Interacting Massive Particles (WIMPs), a promising dark matter candidate. Despite no detection attained yet, the measurements of the current telescopes provide an interesting and competitive constraint on the parameter space [3, 4]. So as to resolve the potential discrepancies on the diffuse emission and to achieve a detection or a definitive rejection against the TeV WIMP paradigm, further advancement of observational research by a next-generation instrument is required.

The Large-Sized Telescope prototype (LST-1), currently under commissioning and taking science data, for the future Cherenkov Telescope Array (CTA) is the next generation of ground-based VHE gamma-ray telescope project, located at a height of 2200 m a.s.l. at the Roque de los Muchachos Observatory in La Palma, Spain (28°N, 18°W). The location requires LST-1 to observe the Galactic Center at the zenith distance (Zd) above about 58° in the horizontal coordinate system. As the technique of the large-zenith-angle observation ($55^\circ \lesssim \text{Zd} \lesssim 70^\circ$) generally engenders telescope responses and shower development different from the standard low zenith angle ($\text{Zd} \lesssim 35^\circ$), additional studies of the technique are needed besides the low-zenith-angle operation. This proceeding presents results from the first LST-1 campaign towards the Galactic Center and those from validation studies of the large-zenith-angle technique for LST-1.

2. Data & Analysis

2.1 Observations and Monte-Carlo Simulations

Two sets of observation data (Data) are used in this study: large zenith angle data on the Crab Nebula taken from December 2020 to March 2023, and large zenith angle data on the Galactic Center taken from April 2021 to June 2022. All the observations were carried out in the so-called wobble mode [5] with the offset angle of 0.4 deg for the Crab Nebula, and 0.5 deg or 0.7 deg for Sgr A*. The total amount of data after data selections is approximately 39 hours and 13 hours for the Galactic Center and the Crab Nebula respectively. Note that this study does not use the stereoscopic-reconstruction technique but only uses data of LST-1 monoscopic observations.

Data analysis of IACTs hinges upon Monte-Carlo (MC) simulations of the atmospheric-shower development and telescope responses. We simulate MCs along trajectories in the horizontal coor-

ordinates of the Galactic Center and the Crab Nebula. In particular, this study uses diffuse MCs for both training and testing in order to extend the analysis in the entire Field of View (FoV).

2.2 Low Level Analysis: Event Reconstruction

Some observation runs of substandard quality, which are affected by inclement weather or hardware malfunction, are excluded from our analysis. The criteria for this selection, based primarily on the cosmic shower rate, are common with the standard low-zenith-angle mode, while making adjustment of thresholds to large zenith angle observations. In data processing, Data and MCs are consistently processed with the official software `cta-lstchain` [6] in accordance with the standard procedure [7]. Based on the so-called Hillas parameters, the Random Forests (RFs) are trained on a point-by-point basis along the trajectories. These RFs are subsequently applied to Data on a run-by-run approach, whose primary objective is to cope with the rapid variations in the telescope response as a function of the zenith and azimuth angles.

Reconstructing an event at the large zenith angle generally poses a difficulty, mainly due to a dimmer and more elongated shower image. This study applies stringent event selections (e.g. events of photo-electrons more than 200 phe are selected.) with the aim at prioritizing the analysis of better-reconstructed events even in the monoscopic operation.

To achieve a robust suppression of the cosmic-ray background, a threshold is imposed on a score `gammanness`, which the RFs yield as a result of the particle-type classification. This study maintains 60% efficiency in gamma-ray MC samples in respective reconstructed energy bins for the purpose of mitigating a significant Data/MC discrepancy. The Data/MC comparison study, as outlined in Sec.3.1, confirms that these relatively strict cuts will not induce a problematic Data/MC discrepancy.

2.3 High Level Analysis: Signal Extraction

Despite the advanced background suppression, the cosmic-ray-induced background persists inexorably, especially at lower energies. In the conventional point-source analysis for data taken in the wobble mode, the reflected-background-region method is widely used to evaluate the irreducible background [8]. In this study, this methodology is also used for analysis of the sources at the wobble center, i.e., Crab Nebula and Sgr A*. By contrast, background estimation for non-central or extended sources requires particular attention. This study employs the exclusion-map technique for an analysis in the E - x - y phase space, which is recently proposed as an advancement of the prior techniques such as the ring-wobble method or the blind-map method [9]. The result is cross-checked with an implementation available in `pybkgmodel` [10].

The final step is to estimate the gamma-ray flux from the excess, which results from the intrinsic gamma-ray flux convolved with the telescope response functions (IRFs). Evaluating the IRFs from the gamma-ray MCs, the intrinsic emission is estimated by performing a forward-folding likelihood fit of spectral and spatial models in `gammapy` [11].

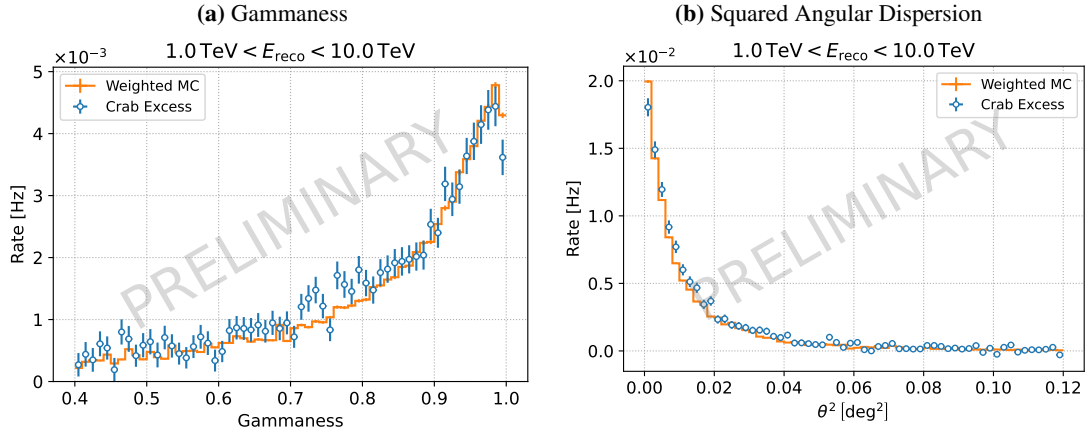


Figure 1: Parameter distributions of the gamma-ray MC simulations and the Crab Nebula data: (a) gammaness and (b) the square of the angular dispersion. For Data the angle θ is defined as the angular distance between the Crab Nebula and an estimated arrival direction, and for MC defined as the angle between true and estimated direction. The gammaness distribution is calculated after a cut of $\theta < 0.1$ deg but before the gammaness cut, whereas the θ^2 plot is obtained without the θ cut but with the 60%-efficiency gammaness cut, whose threshold is between 0.7 and 0.8 depending on the telescope zenith angle. The MC simulation does not include the arcminute-scale fluctuation of the telescope pointing.

3. Results

3.1 Validation of Large-Zenith-Angle MC Simulations

The thorough dependence on the MC simulations in the analysis requires a consistency between MC simulations and actual observations. The large zenith angle observation, in particular, can easily lead to larger Data/MC discrepancies than the standard low zenith angles, as it entails long air-shower development in the rarefied layers of the high-altitude atmosphere. We therefore test our large-zenith-angle MCs by comparing the analytical parameters between MCs and Data of the Crab Nebula.

From Data, a gamma-ray parameter distribution is estimated in analogy of the reflected-background-region technique. The ON region is defined as a circle of a radius of 0.1 deg centered on the Crab Nebula, and two OFF regions are positioned 120 deg apart from the ON region with the pointing position as the center. An excess distribution is obtained by subtracting a histogram in the ON region by those in the OFF regions. As for MC, to convert a histogram into a unit of rate, the gamma-ray MC events are event-by-event re-weighted by the log-parabola energy spectrum reported by MAGIC [12].

Fig.1(a) indicates that the application of the gammaness cuts around 0.7 or 0.8 will not induce a strong bias to the estimation of IRFs, thereby assuring the reliability of the analysis. Fig.1(b) demonstrates the compatible angular resolution between Data and MCs, although a slight broadening effect is noticeable in Data. By fitting the King function, which is regarded as an effective representation of an IACT point spread function [13], the difference in the angular profile between Data and MC is quantified to be about 0.03 deg. This marginal discrepancy may be attributed by the arcminute-scale pointing fluctuations during operation, which are not accounted for the MC simulation.

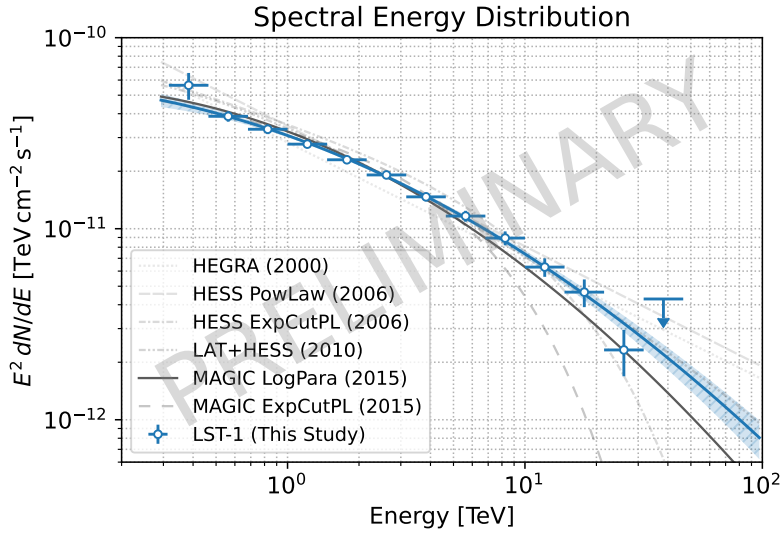


Figure 2: Spectral energy distribution of the Crab Nebula, obtained with the standard spectral analysis of data taken at the large zenith angles. Shown are the data points of the signal-to-background ratio above 5%, the excess above 10, and the Li-Ma significance above 2σ . The vertical error bars show the 1σ statistical uncertainty, the horizontal ones are an energy bin, and the upper limit represents 2σ confidence level. The upper limit is calculated when the excess or significance conditions are not fulfilled but the background events are more than 10 events on top of the satisfied requirement of signal-to-background ratio above 5%.

3.2 Crab Nebula as the Standard Candle for the VHE Gamma Rays

The cross-calibration with other instruments is an indispensable idea for the VHE gamma-ray telescopes including LST-1. Observations of the Crab Nebula, the archetypal plerion, are widely used for this purpose. In this study, the log-parabola function is used to describe the SED: $dN/dE = N_0(E/E_{\text{ref}})^{-\alpha-\beta\log(E/E_{\text{ref}})}$, where $E_{\text{ref}} = 1.0$ TeV. On analysis, the low energy bins below 316 GeV are discarded, where the signal-to-background ratio does not reach 5%.

As shown in Fig.2, the SED in this study is consistent with the previous studies. Notably, a wide energy range between 316 GeV and 31.6 TeV is covered thanks to the combination of the large zenith angle observation and low energy threshold of LST-1. This result demonstrates that the large-zenith-angle observation and analysis of LST-1 is mature enough to carry out scientific research.

3.3 Galactic Center Studies

To begin with, the standard point-source analysis applied for the Crab Nebula is replicated for Sgr A*. The OFF regions are placed at the vertices of the tridecagon only on the outside of the Galactic plane. As with the previous studies, the power-law (PL) model with an exponential cut-off (EC) is used to formulate the SED: $dN/dE = N_0(E/E_{\text{ref}})^{-\alpha} \times \exp(-E/E_{\text{cut}})$.

Furthermore, we extend the analysis to the 3D (E - x - y) phase space. On the estimation of the background, circles of 0.3 deg radius around bright sources (Sgr A* and G0.9+0.1) and a rectangle along the Galactic plane (0.4 deg \times 6.0 deg) are excluded. Fig.3 visualizes clear signals from Sgr A*, G0.9+0.1, and the diffuse emission along the Galactic plane. Although the FoV may include a

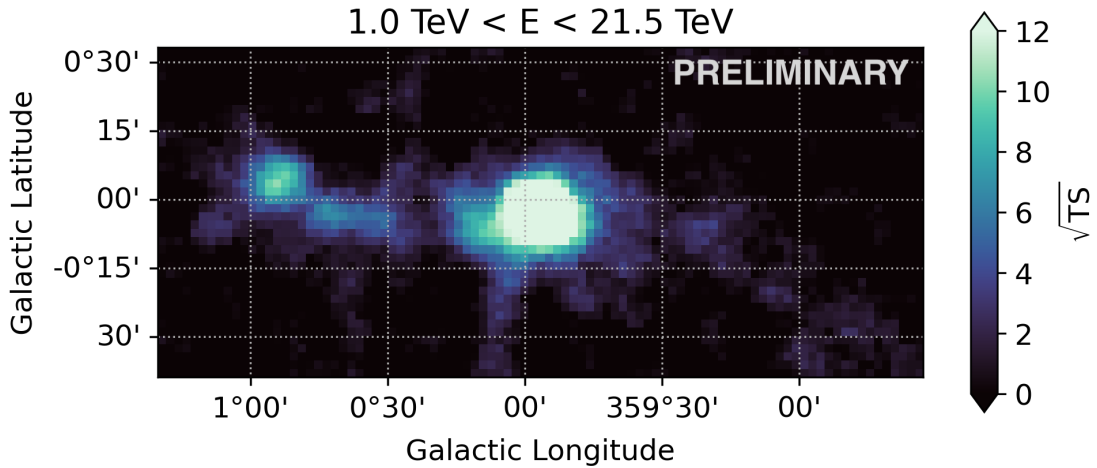


Figure 3: Sky map in the Galactic Center region in units of significance, smeared with a Gaussian of a 0.08 deg standard deviation.

largely extended emission or another point-like gamma-ray source, the current background should cancel out such signals.

Hence, we aim at the characterization of the gamma-ray emission from Sgr A* and G0.9+0.1. ECPL and PL are used for the spectral model, respectively. Regarding the spatial model, a point-source model is assumed for the both sources, while a Gaussian kernel is additionally convolved to the spatial models for the intention to correct for the slight Data/MC discrepancy in the angular resolution as discussed in Sec.3.1. When fitting the models to data, pixels within 0.1 deg from the sources are only used. The spectral parameters are unfrozen with all the parameters in the spatial models fixed. For simplicity, an extended emission is not modeled in this study.

The best-fit models in the 3D analysis are given by $N_0 = (2.62 \pm 0.10) \times 10^{-12} \text{ TeV}^{-1} \text{ cm}^{-2} \text{ s}^{-1}$, $\alpha = 2.14 \pm 0.06$, $E_{\text{cut}} = 20.5^{+8.2}_{-4.6} \text{ TeV}$ for Sgr A*, and $N_0 = (0.58 \pm 0.07) \times 10^{-12} \text{ TeV}^{-1} \text{ cm}^{-2} \text{ s}^{-1}$, $\alpha = 2.30 \pm 0.09$ for G0.9+0.1, where systematic uncertainties are currently not taken into account. Both SEDs are in agreement with the results from the previous measurements, though the cut-off energy of Sgr A* is barely higher.

4. Summary & Outlook

The exploration of the Galactic Center in VHE gamma rays plays an essential role in the spectral and morphological study of the cosmic ray acceleration around the supermassive black hole and in the search for the promising dark matter candidate WIMPs. We present here the results from the first CTA-LST-1 campaign towards the Galactic Center.

This study establishes the large-zenith-angle observation technique for LST-1. The SED of the Crab Nebula, reconstructed from 13 hours of data taken at the large zenith angle, signifies the consistency with previous measurements, covering an energy range between 316 GeV and 31.6 TeV. This wide energy coverage serves to highlight both the low energy threshold of LST-1 and the sensitivity enhanced above TeV by the large-zenith-angle technique.

Drawing upon the successful validation of the technique with the Crab Nebula, the LST-1 Galactic Center data of 39 hours are collected in 2021 and 2022 and are analyzed through our newly developed software. The sky map visualization in Fig.3 highlights prominent signals of Sgr A*, SNR G0.9+0.1, and the diffuse emission along the Galactic plane. The SEDs of the first and second sources, derived from the analysis in the E - x - y phase space, cover the energy range above 464 GeV up to a few tens of TeV, and are in line with results reported by current-generation telescopes.

In conclusion, LST-1 has demonstrated that extended and large-zenith-angle observations are feasible. In order to gain a new insight for the important yet complex region, we will continue to accumulate the Galactic Center data, extend this study to encompass the diffuse emission in the analysis, and design the WIMP search based on the actual LST-1 data.

Acknowledgments

We gratefully acknowledge financial support from the following agencies and organisations:
CTA Consortium: https://www.cta-observatory.org/consortium_acknowledgments/
CTA-LST Project: <https://www.lst1.iac.es/acknowledgements.html>

References

- [1] HESS Collaboration, *Acceleration of petaelectronvolt protons in the galactic centre*, *Nature* **531** (2016) 476.
- [2] MAGIC Collaboration, Acciari, V. A., Ansoldi, S., Antonelli, L. A., Arbet Engels, A., Baack, D. et al., *Magic observations of the diffuse emission in the vicinity of the galactic center*, *A&A* **642** (2020) A190.
- [3] H.E.S.S. COLLABORATION collaboration, *Search for dark matter annihilation signals in the h.e.s.s. inner galaxy survey*, *Phys. Rev. Lett.* **129** (2022) 111101.
- [4] MAGIC COLLABORATION collaboration, *Search for gamma-ray spectral lines from dark matter annihilation up to 100 tev toward the galactic center with magic*, *Phys. Rev. Lett.* **130** (2023) 061002.
- [5] V.P. Fomin, A.A. Stepanian, R.C. Lamb, D.A. Lewis, M. Punch and T.C. Weekes, *New methods of atmospheric Cherenkov imaging for gamma-ray astronomy. I. The false source method*, *Astroparticle Physics* **2** (1994) 137.
- [6] R. Lopez-Coto, T. Vuillaume, A. Moralejo, F. Cassol, M. Linhoff, C. Priyadarshi et al., *cta-observatory/cta-lstchain: v0.9.9 - 2022-10-25*, Oct., 2022. 10.5281/zenodo.7249299.
- [7] CTA-LST Project, S. Abe, A. Aguasca-Cabot, I. Agudo, N.A. Crespo, L.A. Antonelli et al., *Observations of the crab nebula and pulsar with the large-sized telescope prototype of the cherenkov telescope array*, 2023.
- [8] F. Aharonian, A. Akhperjanian, J. Barrio, K. Bernlöhner, H. Börsch, H. Bojahr et al., *Evidence for TeV gamma ray emission from Cassiopeia A*, *A&A* **370** (2001) 112 [[astro-ph/0102391](https://arxiv.org/abs/astro-ph/0102391)].

- [9] I. Vovk, M. Strzys and C. Fruck, *Spatial likelihood analysis for MAGIC telescope data. From instrument response modelling to spectral extraction*, *A&A* **619** (2018) A7 [1806.03167].
- [10] Marcel C. Strzys, Ievgen Vovk, Moritz Hütten, Mathieu de Bony de Lavergne, Simone Mender and Shotaro Abe, *Pybkgmodel - a background modelling toolbox for the cta*, in *Proceedings of 38th International Cosmic Ray Conference — PoS(ICRC2023)*, jul, 2023.
- [11] A. Donath, C. Deil, R. Terrier, J.E. Ruiz, J. King, Q. Remy et al., *Gammapy: Python toolbox for gamma-ray astronomy*, May, 2022. 10.5281/zenodo.6552377.
- [12] J. Aleksić, S. Ansoldi, L. Antonelli, P. Antoranz, A. Babic, P. Bangale et al., *Measurement of the crab nebula spectrum over three decades in energy with the magic telescopes*, *Journal of High Energy Astrophysics* **5-6** (2015) 30.
- [13] P. Da Vela, A. Stamerra, A. Neronov, E. Prandini, Y. Konno and J. Sitarek, *Study of the IACT angular acceptance and Point Spread Function*, *Astroparticle Physics* **98** (2018) 1.

Full Author List: The CTA-LST Project

K. Abe¹, S. Abe², A. Aguasca-Cabot³, I. Agudo⁴, N. Alvarez Crespo⁵, L. A. Antonelli⁶, C. Aramo⁷, A. Arbet-Engels⁸, C. Arcaro⁹, M. Artero¹⁰, K. Asano², P. Aubert¹¹, A. Baktash¹², A. Bamba¹³, A. Baquero Larriva^{5,14}, L. Baroncelli¹⁵, U. Barres de Almeida¹⁶, J. A. Barrio⁵, I. Batković⁹, J. Baxter², J. Becerra González¹⁷, E. Bernardini⁹, M. I. Bernardos⁴, J. Bernete Medrano¹⁸, A. Berti⁸, P. Bhattacharjee¹¹, N. Biederbeck¹⁹, C. Bigongiari⁶, E. Bissaldi²⁰, O. Blanch¹⁰, G. Bonnoli²¹, P. Bordas³, A. Bulgarelli¹⁵, I. Burelli²², L. Burmistrov²³, M. Buscemi²⁴, M. Cardillo²⁵, S. Caroffi¹¹, A. Carosi⁶, M. S. Carrasco²⁶, F. Cassol²⁶, D. Cauz²², D. Cerasole²⁷, G. Ceribella⁸, Y. Chai⁸, K. Cheng², A. Chiavassa²⁸, M. Chikawa², L. Chytka²⁹, A. Cifuentes¹⁸, J. L. Contreras⁵, J. Cortina¹⁸, H. Costantini²⁶, M. Dalchenko²³, F. Dazzi⁶, A. De Angelis⁹, M. de Bony de Lavergne¹¹, B. De Lotto²², M. De Lucia⁷, R. de Menezes²⁸, L. Del Peral³⁰, G. Deleglise¹¹, C. Delgado¹⁸, J. Delgado Mengual³¹, D. della Volpe²³, M. Dellaiera¹¹, A. Di Piano¹⁵, F. Di Piero²⁸, A. Di Pilato²³, R. Di Tria²⁷, L. Di Venere²⁷, C. Díaz¹⁸, R. M. Dominik¹⁹, D. Dominis Prester³², A. Donini⁶, D. Dorner³³, M. Doró⁹, L. Eisenberger³³, D. Elsässer¹⁹, G. Emery²⁶, J. Escudero⁴, V. Fallah Ramazani³⁴, G. Ferrara²⁴, F. Ferraro³⁵, A. Fiasson^{11,36}, L. Foffano²⁵, L. Freixas Coromina¹⁸, S. Fröse¹⁹, S. Fukami², Y. Fukazawa³⁷, E. García¹¹, R. García López¹⁷, C. Gasbarra³⁸, D. Gasparrini³⁸, D. Geyer¹⁹, J. Giesbrecht Paiva¹⁶, N. Giglietto²⁰, F. Giordano²⁷, P. Gliwny³⁹, N. Godinovic⁴⁰, R. Grau¹⁰, J. Green⁸, D. Green⁸, S. Gunji⁴¹, P. Günther³³, J. Hackfeld³⁴, D. Hadasch², A. Hahn⁸, K. Hashiyama², T. Hassan¹⁸, K. Hayashi², L. Heckmann⁸, M. Heller²³, J. Herrera Lorente¹⁷, K. Hirotani², D. Hoffmann²⁶, D. Horns¹², J. Houles²⁶, M. Hrabovsky²⁹, D. Hrupec⁴², D. Hui², M. Hütten², M. Iarlori⁴³, R. Imazawa³⁷, T. Inada², Y. Inome², K. Ioka⁴⁴, M. Iori³⁵, K. Ishio³⁹, I. Jimenez Martinez¹⁸, J. Jurysek⁴⁵, M. Kagaya², V. Karas⁴⁶, H. Katagiri⁴⁷, J. Kataoka⁴⁸, D. Kerszberg¹⁰, Y. Kobayashi², K. Kohri⁴⁹, A. Kong², H. Kubo², J. Kushida¹, M. Lainez⁵, G. Lamanna¹¹, A. Lamastra⁶, T. Le Flour¹¹, M. Linhof¹⁹, F. Longo⁵⁰, R. López-Coto⁴, A. López-Oramas¹⁷, S. Loporchio²⁷, A. Lorini⁵¹, J. Lozano Bahilo³⁰, P. L. Luque-Escamilla⁵², P. Majumda^{53,2}, M. Makariev⁵⁴, D. Mandat⁴⁵, M. Manganaro³², G. Manico²⁴, K. Mannheim³³, M. Mariotti⁹, P. Marquez¹⁰, G. Marsella^{24,55}, J. Martí⁵², O. Martínez⁵⁶, G. Martínez¹⁸, M. Martínez¹⁰, A. Mas-Aguilar⁵, G. Maurin¹¹, D. Mazin^{2,8}, E. Mestre Guillen⁵², S. Micanovic⁵², D. Miceli⁹, T. Miener⁵, J. M. Miranda⁵⁶, R. Mirzoyan⁸, T. Mizuno⁵⁷, M. Molero Gonzalez¹⁷, E. Molina³, T. Montaruli²³, I. Monteiro¹¹, A. Moralejo¹⁰, D. Morcuende⁵, A. Morselli³⁸, V. Moya⁵, H. Murai⁵⁸, K. Murase², S. Nagataki⁵⁹, T. Nakamori⁴¹, A. Neronov⁶⁰, L. Nickel¹⁹, M. Nieves Rosillo¹⁷, K. Nishijima¹, K. Noda², D. Nosek⁶¹, S. Nozaki⁸, M. Ohishi², Y. Ohtani², T. Oka⁶², A. Okumura^{63,64}, R. Orito⁶⁵, J. Otero-Santos¹⁷, M. Palatiello²², D. Paneque⁸, F. R. Pantaleo²⁰, R. Paoletti⁵¹, J. M. Paredes³, M. Pech^{45,29}, M. Pecimotika³², M. Peresano²⁸, F. Pfeiffle³³, E. Pietropaolo⁶⁶, G. Pirola⁹, C. Plard¹¹, F. Podobnik²¹, V. Poireau¹¹, M. Polo¹⁸, E. Pons¹¹, E. Prandini⁹, J. Prast¹¹, G. Principe³⁰, C. Priyadarshi¹⁰, M. Prouza⁴⁵, R. Rando⁹, W. Rhode¹⁹, M. Ribó³, C. Righi²¹, V. Rizzi⁶⁶, G. Rodríguez Fernández³⁸, M. D. Rodríguez Frías³⁰, T. Saito², S. Sakurai², D. A. Sanchez¹¹, T. Sarić⁴⁰, Y. Sato⁶⁷, F. G. Saturni⁶, V. Savchenko⁶⁰, B. Schleiher³³, F. Schmuckermair⁸, J. L. Schuber¹⁹, F. Schussler⁶⁸, T. Schweizer⁸, M. Seglar Arroyo¹¹, T. Siegert³³, R. Silva²⁷, J. Sitarek³⁹, V. Sliusar⁶⁹, A. Spolon⁹, J. Strišković⁴², M. Strzys², Y. Suda³⁷, H. Tajima⁶³, M. Takahashi⁶³, H. Takahashi³⁷, J. Takata², R. Takeishi², P. H. T. Tam², S. J. Tanaka⁶⁷, D. Tateishi⁷⁰, P. Temnikov⁵⁴, Y. Terada¹⁰, K. Terauchi⁶², T. Terzić³², M. Teshima^{8,2}, M. Tluczykont¹², F. Tokana⁴¹, D. F. Torres⁷¹, P. Travnicek⁴⁵, S. Truzzi⁵¹, A. Tutone⁶, M. Vacula²⁹, P. Vallania²⁸, J. van Scherpenberg⁸, M. Vázquez Acosta¹⁷, I. Vial⁹, A. Vigliano²², C. F. Vigorito^{28,72}, V. Vitale³⁸, G. Voutsinas²³, I. Vovk², T. Vuillaume¹¹, R. Walter⁶⁹, Z. Wei⁷¹, M. Will⁸, T. Yamamoto⁷³, R. Yamazaki⁶⁷, T. Yoshida⁴⁷, T. Yoshikoshi², N. Zywicka³⁹

¹Department of Physics, Tokai University. ²Institute for Cosmic Ray Research, University of Tokyo. ³Departament de Física Quàntica i Astrofísica, Institut de Ciències del Cosmos, Universitat de Barcelona, IEEC-UB. ⁴Instituto de Astrofísica de Andalucía-CSIC. ⁵EMFTEL department and IPARCOS, Universidad Complutense de Madrid. ⁶INAF - Osservatorio Astronomico di Roma. ⁷INFN Sezione di Napoli. ⁸Max-Planck-Institut für Physik. ⁹INFN Sezione di Padova and Università degli Studi di Padova. ¹⁰Institut de Física d'Altes Energies (IFAE), The Barcelona Institute of Science and Technology. ¹¹LAPP, Univ. Grenoble Alpes, Univ. Savoie Mont Blanc, CNRS-IN2P3, Annecy. ¹²Universität Hamburg, Institut für Experimentalphysik. ¹³Graduate School of Science, University of Tokyo. ¹⁴Universidad del Azuay. ¹⁵INAF - Osservatorio di Astrofisica e Scienza dello spazio di Bologna. ¹⁶Centro Brasileiro de Pesquisas Físicas. ¹⁷Instituto de Astrofísica de Canarias and Departamento de Astrofísica, Universidad de La Laguna. ¹⁸CIEMAT. ¹⁹Department of Physics, TU Dortmund University. ²⁰INFN Sezione di Bari and Politecnico di Bari. ²¹INAF - Osservatorio Astronomico di Brera. ²²INFN Sezione di Trieste and Università degli Studi di Udine. ²³University of Geneva - Département de physique nucléaire et corpusculaire. ²⁴INFN Sezione di Catania. ²⁵INAF - Istituto di Astrofisica e Planetologia Spaziali (IAPS). ²⁶Aix Marseille Univ, CNRS/IN2P3, CPPM. ²⁷INFN Sezione di Bari and Università di Bari. ²⁸INFN Sezione di Torino. ²⁹Palacky University Olomouc, Faculty of Science. ³⁰University of Alcalá UAH. ³¹Port d'Informació Científica. ³²University of Rijeka, Department of Physics. ³³Institute for Theoretical Physics and Astrophysics, Universität Würzburg. ³⁴Institut für Theoretische Physik, Lehrstuhl IV: Plasma-Astroteilchenphysik, Ruhr-Universität Bochum. ³⁵INFN Sezione di Roma La Sapienza. ³⁶ILANCE, CNRS. ³⁷Physics Program, Graduate School of Advanced Science and Engineering, Hiroshima University. ³⁸INFN Sezione di Roma Tor Vergata. ³⁹Faculty of Physics and Applied Informatics, University of Lodz. ⁴⁰University of Split, FESB. ⁴¹Department of Physics, Yamagata University. ⁴²Josip Juraj Strossmayer University of Osijek, Department of Physics. ⁴³INFN Dipartimento di Scienze Fisiche e Chimiche - Università degli Studi dell'Aquila and Gran Sasso Science Institute. ⁴⁴Yukawa Institute for Theoretical Physics, Kyoto University. ⁴⁵FZU - Institute of Physics of the Czech Academy of Sciences. ⁴⁶Astronomical Institute of the Czech Academy of Sciences. ⁴⁷Faculty of Science, Ibaraki University. ⁴⁸Faculty of Science and Engineering, Waseda University. ⁴⁹Institute of Particle and Nuclear Studies, KEK (High Energy Accelerator Research Organization). ⁵⁰INFN Sezione di Trieste and Università degli Studi di Trieste. ⁵¹INFN and Università degli Studi di Siena, Dipartimento di Scienze Fisiche, della Terra e dell'Ambiente (DSFTA). ⁵²Escuela Politécnica Superior de Jaén, Universidad de Jaén. ⁵³Saha Institute of Nuclear Physics. ⁵⁴Institute for Nuclear Research and Nuclear Energy, Bulgarian Academy of Sciences. ⁵⁵Dipartimento di Fisica e Chimica 'E. Segrè' Università degli Studi di Palermo. ⁵⁶Grupo de Electronica, Universidad Complutense de Madrid. ⁵⁷Hiroshima Astrophysical Science Center, Hiroshima University. ⁵⁸School of Allied Health Sciences, Kitasato University. ⁵⁹RIKEN, Institute of Physical and Chemical Research. ⁶⁰Laboratory for High Energy Physics, École Polytechnique Fédérale. ⁶¹Charles University, Institute of Particle and Nuclear Physics. ⁶²Division of Physics and Astronomy, Graduate School of Science, Kyoto University. ⁶³Institute for Space-Earth Environmental Research, Nagoya University. ⁶⁴Kobayashi-Maskawa Institute (KMI) for the Origin of Particles and the Universe, Nagoya University. ⁶⁵Graduate School of Technology, Industrial and Social Sciences, Tokushima University. ⁶⁶INFN Dipartimento di Scienze Fisiche e Chimiche - Università degli Studi dell'Aquila and Gran Sasso Science Institute. ⁶⁷Department of Physical Sciences, Aoyama Gakuin University. ⁶⁸IRFU, CEA, Université Paris-Saclay. ⁶⁹Department of Astronomy, University of Geneva. ⁷⁰Graduate School of Science and Engineering, Saitama University. ⁷¹Institute of Space Sciences (ICE-CSIC), and Institut d'Estudis Espacials de Catalunya (IEEC), and Institutio Catalana de Recerca i Estudis Avançats (ICREA). ⁷²Dipartimento di Fisica - Università degli Studi di Torino. ⁷³Department of Physics, Konan University.